

# Corrosion Degradation of AXJ530 Magnesium Alloy in Simulated Physiological Fluid and Its Mitigation by Fluoride and Chitosan Coatings for Osteosynthetic Applications

Fakiha El-Taib Heakal\* and Amira M. Bakry

Chemistry Department, Faculty of Science, Cairo University, Giza 12613, Egypt.

\*E-mail: [feltaibheakal@gmail.com](mailto:feltaibheakal@gmail.com); [fakihheakal@yahoo.com](mailto:fakihheakal@yahoo.com); [hfakiha@sci.cu.edu.eg](mailto:hfakiha@sci.cu.edu.eg)

Received: 9 April 2018 / Accepted: 1 June 2018 / Published: 5 July 2018

---

The *in vitro* corrosion behavior of a new Ca-containing Mg alloy (AXJ530) was investigated in phosphate buffer saline (PBS) solution of pH 7.4 at 37 °C for potential biodegradable implant applications. Chemical methods as well as electrochemical open circuit potential, EIS and potentiodynamic polarization techniques were used to assess its vulnerability in PBS with time lapse over 96 h. The results showed that the corrosion rate is always faster for the alloy than for pure Mg at any immersion time > 3 h, mainly due to the micro-galvanic coupling effect. An important factor for Mg alloy application as biodegradable implant is the enhancement of its corrosion resistance and biocompatibility. To achieve this goal, the effect of hydrofluoric acid treatment on the corrosion performance of the alloy was examined by steeping the sample first in sodium hydroxide then in 40 wt.% HF solutions for 24 h at room temperature. Also, coated samples with chitosan (CS) natural polymer were performed using spin coating technique to improve the durability of the alloy. The electrochemical tests revealed that two-layer CS coating can effectively reduce the alloy deterioration in PBS and hence increases its biocompatibility compared to the HF-treated or the untreated bare alloy samples. Additionally, the sample surface of the alloy compared to that for Mg, before and after 96 h immersion in PBS were also examined by using SEM and EDX analyses to support the above obtained experimental results.

---

**Keywords:** Magnesium alloy; Biomaterials; Corrosion; Coatings; Fluoride; Chitosan; EIS.

## 1. INTRODUCTION

Metals and their alloys whose ions already exist in our bodies are considered promising candidates for biomedical applications such as load bearing orthopedic implants and coronary stents. In this regard, magnesium and its alloys have enticed much attention as implants with a temporary function, such as stents and plates offering temporary mechanical support as they corrode completely

after tissue healing. This is because of the different roles played by the naturally existing  $Mg^{2+}$  ions in our biological systems [1]. Besides, magnesium alloys are the lightest among other structural materials and their elastic modules as well as their compressive yield strength are closer to those of human bone than other medical implants (Table 1) [2,3]. Accordingly, magnesium based materials are potentially considered for osteosynthetic applications. In addition, their natural biodegradability avoids saves the need of a second surgical procedure after tissue healing. On the other hand, since Mg is found in bone tissue [4], and being the second most abundant intracellular cation [5], released Mg ions serve as an important element in human metabolism. Unfortunately, magnesium alloys are very reactive in local environment and corrode rapidly at physiological pH and temperature leading to defect in the mechanical integrity before a substantial tissue healing occurs [1]. Therefore, it is essential to closely diminish the corrosion rate of magnesium alloys in body environment, especially when it is employed for orthopedic implant applications. Moreover, various alloying elements are merged into Mg to improve its mechanical properties and/or corrosion resistance. Those elements influence the final material structure and impact its corrosion performance, corrosion resistance, surface morphology and biocompatibility. However, in biomedical applications, the cytotoxicity of these alloying elements needs to be elucidated. Corrosion induced cytotoxicity is mainly related to its corrosion products containing dissolved ions and precipitated corrosion debris on the implant surface. Up to date, some magnesium alloys such as Al-Zn containing alloys, *e.g.* AZ91 and AZ31 [6], rare earth containing alloys, *e.g.* WE43 and LAE442 [7], as well as Ca-containing magnesium alloys [8], have been proposed for orthopedic applications.

**Table 1.** Physical and mechanical properties of biomedical magnesium and some magnesium alloys in comparison with natural bone [3].

Properties	Natural bone	Mg-cast	AZ91D die cast	AZ31 extruded	Mg-1Ca Extruded
Density ( $g/cm^3$ )	1.8–2.0	1.74	1.81	1.78	-
Compressive yield strength (MPa)	164-240	-	160	60-70	-
Ultimate tensile strength (MPa)	35-283	86.8±2.5	230	235	239.6±7.2
Elastic modulus (GPa)	5-23	41	45	45	-
Yield strength (MPa)	104.9-114.3	20.9±2.3	150	125-135	135.6±5.4

Calcium in particular which is the main element in human bone has been recently identified as one of the alloying elements for magnesium to improve bone healing through dual release of magnesium and calcium ions [8]. By adding Ca, there is more advantage of increasing the low ignition temperature of the molten Mg alloys caused by the formation of a stable oxide film [9]. Furthermore, Ca addition to Mg-Al based alloys leads to improve creep resistance of the alloy due to formation of  $(Mg,Al)_2Ca$  phases. In this regard, Powell et al. [10] have revealed two important findings concerning Mg-Al-Ca (AX) alloy system. (i) Casting defects such as hot-cracking, cold-shuts, and die-sticking of AX alloys were very severe when Ca level is about 1%. However, such problems diminished or significantly reduced when Ca levels were about 2%. (ii) Additions of about 0.1% strontium to Mg-Al-Ca alloys further improved their creep resistance. Strontium (Sr) additions are also beneficial to the corrosion resistance of the alloys and could effectively restore the corrosion resistance to the level of AZ91D alloy.

Based on the above findings, a family of Mg-Al-Ca-Sr (AXJ) alloys was developed including AXJ530 which is a creep-resistant magnesium alloy with a nominal composition of Mg–5 wt.% Al–3 wt.% Ca– 0.15 wt.% Sr [11,12]. To the best of our knowledge, there is only very limited studies on the corrosion resistance of AXJ530 alloy and even no work has been done concerning its corrodibility under physiological conditions. Increasing corrosion resistance is a key role in enhancing Mg alloys implants as biocompatible load-bearing ones. In this respect, several reports have shown that reducing the corrosion rate of Mg materials in simulated body fluids is possible by surface treatment methods such as conversion coatings [13], hydride coatings [14], alkali-heat-treatment [15], anodizing [16], polymeric coatings [17] and electrodeposition [18]. Among those approaches, chemical conversion coating via hydrofluoric acid treatment is considered as a promising option owing to its simplicity and low cost of application. By applying this method, a protective layer from magnesium fluoride ( $\text{MgF}_2$ ) is developed on the substrate surface which serves as a physical barrier preventing its reaction with the contacting environment. The  $\text{MgF}_2$  coating has also been reported to provide high density layer which is chemically inert and non-toxic as fluorine is known to be among human bone and teeth components [19]. The integrity of the coating is correlated to the chemical and mechanical stability of the implant in the physiological fluid. Therefore, in order to achieve a more efficient barrier, coating the alloy sample was steeped first in hydrofluoric acid followed by post-coat the fluoride layer with chitosan natural polymer using spin coating technique that is commonly adopted for producing thin polymer film with a homogeneous thickness. A typical process involved depositing the polymer solution onto a solid substrate and then start rotating the substrate at high speed. Due to spinning, the solvent evaporated leaving a residual solid polymer film covering the substrate surface [20]. Chitosan, an interesting natural polysaccharide, being a widely used material for coatings aimed at improving hydrophobicity, biocompatibility and microbial resistance [21,22]. The present study is mainly intended to understand the behavior of a new magnesium alloy (AXJ530) in simulated physiological fluid (PBS) of pH 7.4 at the average human body temperature of 37 °C relative to its base metal (Mg) as a control. While this metallic alloy is highly beneficial since it contains two essential elements to our bodies (Ca and Sr), it dissolves too quickly inside the human body which is highly detrimental to patients. Therefore, improving the alloy corrosion resistance was also our main important task that was achieved by using fluoride and chitosan coating regimes in order to control its performance as a potential biodegradable medical implant. Chemical methods as well as electrochemical open circuit potential, EIS and potentiodynamic polarization techniques were used to assess its vulnerability in PBS over time lapse extended to 96 h. For better understanding the obtained results, SEM micrographs and EDX examinations were also used to correlate the electrochemical behavior with the alloy surface microstructure and its elemental composition.

## 2. EXPERIMENTAL

### 2.1. Materials and electrodes

The materials used in the present work were extruded AXJ530 alloy and pure Mg (99.94%) with chemical compositions as listed in Table 2. Commonly, extruded magnesium alloys have wide applications due to their proper ductility, good plasticity and fine homogeneous microstructure and

particle distributions. Materials were cut into coupons, encapsulating each one into a glass tube with an epoxy resin leaving unveiled surface area of 0.250 and 0.264 cm<sup>2</sup> for pure Mg and the alloy to face the solution. Prior to each experiment the working electrode was mechanically ground using successively finer grades of emery papers from 600 to 1500 grit until mirror finish then smoothing the surface with fine filter paper, degreased with acetone, rinsed with deionized water and air dried before immersed quickly into the test medium under aerated quiescent conditions.

## 2.2. Test medium and surface morphology

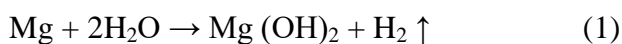
All experiments were scrutinized with time after immersing each sample in the test phosphate buffer saline (PBS) fluid of composition (in g/L) as [23]: 8.006 NaCl, 0.201 KCl, 0.240 KH<sub>2</sub>PO<sub>4</sub> and 1.420 Na<sub>2</sub>HPO<sub>4</sub> (pH 7.4) at 37 ± 0.2 °C. They were prepared from analytical grade chemicals without further purification using deionized water. To observe the surface morphologies of the examined specimens after various experimental treatments, SEM micrographs were collected using Quanta 250 FEG (Field Emission Gun) equipped with EDX Unit (Energy Dispersive X-ray Analyzer), with accelerating voltage 30 kV and magnification 14× up to 1000 000× and resolution for Gun 1nm (FEI company, Netherlands). Each experiment was carried out three times to check the reproducibility of results.

**Table 2.** Chemical composition (wt.%) of AXJ530 alloy and Mg metal.

Element	Al	Zn	Ca	Sr	Mn	Si	Fe	Cu	Ni	Be	Mg
<b>AXJ530</b>	4.7	-	2.6	0.15	0.3	-	0.002	<0.003	<0.002	-	Bal.
<b>Mg</b>	0.005	-	-	-	0.002	-	0.03	0.002	0.001	-	Bal.

## 2.3. Chemical methods

The average degradation rates of AXJ530 alloy samples after immersion in PBS for different time periods were determined using hydrogen evolution and weight loss measurements at constant temperature of 37 ± 0.2 °C inside an air thermostat. In the hydrogen evolution method the specimen was soaked in PBS with a volume/area ratio of 25 mL/1 cm<sup>2</sup> for time lapse extended up to 96 h. The degradation rate was evaluated by measuring the volume of evolved hydrogen gas collected in a burette filled with PBS solution and mounted on an inverted funnel placed over the specimen. The evolved hydrogen is a direct measure of the degradation rate based on the following balanced overall corrosion process, where one molecule of hydrogen gas is evolved for each Mg atom dissolved from the sample:



The corresponding rate of hydrogen evolved,  $V_{\text{H}}$  (mL cm<sup>-2</sup> d<sup>-1</sup>) was then obtained from the following relation:

$$V_{\text{H}} = \frac{v_t}{st} \quad (2)$$

where  $v_t$  is the volume of hydrogen gas at time  $t$  and  $s$  is the sample exposed surface area. The degradation rate was also determined from the chemical method by the weight loss measurement according to ASTM G31-72. The specimens were immersed in PBS with a volume/area ratio of 25 mL/1 cm<sup>2</sup> for different time periods of 10 h, 96 h, 168 h and 360 h. Separate specimens were used to determine the weight loss for each exposure period. Prior to the commencement of each immersion test, the specimen was abraded progressively by finer grade of emery papers up to 1500 grit finish and then weighed. All immersion tests were carried out without disturbing the corroding system at 37 ± 0.2 °C. The corroded specimens were removed from the test solution after a definite immersion period, cleaned several times with distilled water to remove the corrosion products and then left to dry in a desiccator. The dried specimen was weighed and the degradation rate,  $\Delta w$  (mg cm<sup>-2</sup> d<sup>-1</sup>) was calculated as follows:

$$\Delta w = \frac{m_a - m_b}{st} \quad (3)$$

where  $m_a$  and  $m_b$  represent the sample mass before and after immersion.

#### 2.4. Electrochemical methods

All electrochemical measurements were conducted at 37 °C using the electrochemical workstation IM6e Zahner-elektrok, Koronach, Germany, controlled by Thales software. Experiments were performed in a standard three-electrode glass cell furnished with a large platinum sheet (2.0 cm × 4.0 cm × 0.2 cm) and AXJ530 alloy or pure Mg to serve as counter and working electrodes, respectively. A saturated calomel electrode (SCE) was used as a reference for all potential measurements ( $E_{SCE} = 0.241$  V vs SHE). Potentiodynamic polarization scans were recorded at a rate of 2 mV s<sup>-1</sup>. EIS was conducted at the open-circuit potential (OCP) after different exposure periods extended up to 96 h, by applying an excitation ac signal of 10 mV peak to peak in the frequency domain of 30 kHz down to 10 mHz with eight to five points per decade. The EIS data were simulated using Thales software and an appropriate equivalent electronic circuit model. Corrosion current density ( $i_{corr}$ ) which is equivalent to the corrosion rate of the specimen is given by the intersection of the cathodic Tafel line with the pre-determined free corrosion potential ( $E_{corr}$ ), namely to the potential at which the anodic and cathodic reactions at the working electrode/solution interface were balanced using Thales software for  $I-E$  analysis. In all cases, the tests were performed in triplicate using a new surface and fresh solution to guarantee the reliability of the results.

#### 2.5. Surface protection

##### 2.5.1. Fluoride conversion coating

For the chemical conversion coating surface, pre-treatment is an important issue to help to functionalize the substrate and thus facilitates the coating process to develop a stronger and more stable coat. Accordingly, the abraded AXJ530 alloy specimens were first washed entirely with deionized water, ultrasonically degreased with ethanol and dried in a warm stream of air. The specimens were then etched in 25 wt.% NaOH solution for 2 h, followed by a cleaning step with

deionized water and air drying. After that, they were steeped into 40 wt.% HF for 24 h at room temperature. Finally, the treated specimens were washed with deionized water, dried and subsequently checked visually for the uniformity of coated fluoride layers before characterization.

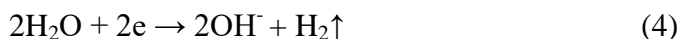
### 2.5.2. Chitosan coating

Spin-coated chitosan films on the HF-treated specimens of AXJ530 alloy were performed using chitosan and acetic acid solutions. The chitosan solution was prepared by dissolving the as-received chitosan (with de-acetylation degree of 95%) at 2.5 wt.% in 5 mL of 50 wt.% acetic acid solution in water [24]. The chitosan was allowed to dissolve ultrasonically for 1 h at room temperature. One drop of chitosan solution was spread on the alloy surface and spin coated with a maximum speed of 1500 rpm for 30 s. After that, the sample was left to dry at 60 °C for 20 min. before applying another layer. This two-step sequential method was repeated 2 and 6 times to enable tailoring coated specimens with 2 and 6 layers, respectively. Finally, the coated specimens were left to dry at 60 °C under vacuum for 24 h before characterization.

## 3. RESULTS AND DISCUSSION

### 3.1. Immersion testing

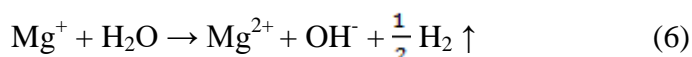
The immersion corrosion tests are the simplest of the *in vitro* methods for investigating the degradation performance of Mg materials, which has led to their relative popularity. Interestingly, in neutral/alkaline media cathodic hydrogen evolution (HE) occurs on magnesium based sample well above the open circuit potential *via* water reduction:



This is because dissolution potentials of magnesium materials at all pH values are sufficiently less than about -1.45 V (vs. SCE), whereby HE dominates the oxygen reduction [25]. Accordingly, under open circuit conditions  $\text{Mg}^{2+}$  cation release from the sample in near neutral aqueous solutions is always accompanied by copious HE. Additionally, several authors have suggested that Mg could be dissolved as unipositive ion ( $\text{Mg}^+$ ) as follows [26,27]:



The monovalent cation will subsequently hydrolyze in water *via* a secondary chemical reaction (Eq.6) spawning an excessive hydrogen gas evolution [26]:



As such, the degradation rates of the tested magnesium material can be monitored by measuring the HE rates, since the corrosion products do not influence the relationship between HE and the release of Mg cations. Therefore, hydrogen evolution method would be reliable, easy to implement and not liable to errors relevant to weight loss measurement, despite that both are considered the simplest and well established methods for estimating corrosion rates of several materials [28]. Fig. 1 depicts the variation with time of the HE rate ( $V_{\text{H}} / \text{mL cm}^{-2} \text{d}^{-1}$ ) for the alloy steeped in PBS fluid at 37 °C. As it can be seen, in the early immersion stage  $V_{\text{H}}$  is very high and drops rapidly during the first 3 h

of immersion but decreases slowly in the later stage until almost stabilizes after a critical immersion time of ~ 9 h realizing 2.69 and 2.55 mL cm<sup>-2</sup> d<sup>-1</sup> after 10 and 96 h, respectively. Higher volume of HE at the early stages of immersion were previously noted by several authors *in vitro* and *in vivo* studies [7,29-31]. From the mass loss method, the average weight loss rate of AXJ530 alloy after immersion in PBS fluid for 10 h was found to be 2.52 mg cm<sup>-2</sup> d<sup>-1</sup>. This value increases to 11.95 mg cm<sup>-2</sup> d<sup>-1</sup> after 96 h immersion and continued increasing to 19.85 mg cm<sup>-2</sup> d<sup>-1</sup> after 168 h to reach a value of 28.3 mg cm<sup>-2</sup> d<sup>-1</sup> at the end of 360 h immersion. The high corrosion rate of AXJ530 alloy in PBS fluid is likely related to the presence of chloride and phosphate ions, where aggressive Cl<sup>-</sup> ions in the medium pose the biggest threat [28]. Chloride ions can transform the partially protective Mg(OH)<sub>2</sub> layer into more soluble MgCl<sub>2</sub> rendering the surface to be more vulnerable to corrosion by reducing its protected area, and thus further dissolution of magnesium is enhanced. Song et al [28]. also suspect that chloride ions are involved in the intermediate step of magnesium dissolution by accelerating the electrochemical reaction rate from magnesium to magnesium univalent ions (Eq.(5)) which reacts with water to produce Mg<sup>2+</sup> (Eq. (6)). This lead to the formation of the following product [31]:

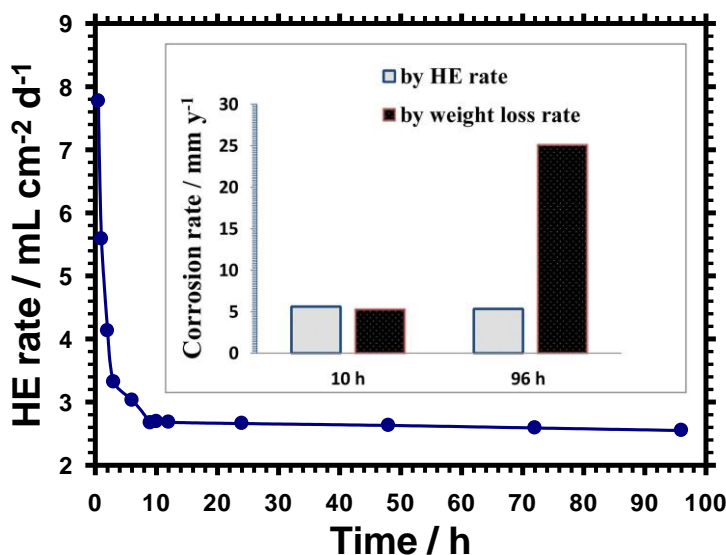
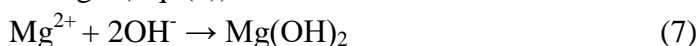
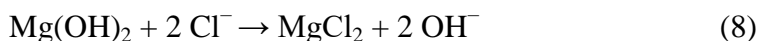


**Figure 1.** HE rate in mL cm<sup>-2</sup> d<sup>-1</sup> and weight loss rate in mm y<sup>-1</sup> (inset) for the alloy as a function of the immersion time.

Nonetheless, in presence of adsorbed Cl<sup>-</sup> ions on the surface Mg(OH)<sub>2</sub> can be readily transferred to the more soluble MgCl<sub>2</sub> *via* the following reaction:



Direct formation of MgCl<sub>2</sub> according to Eq. (9) cannot be also excluded:



Additionally, precipitation of Mg<sub>3</sub>(PO<sub>4</sub>)<sub>2</sub> consumes OH<sup>-</sup> ions and hence can stimulate the release of Mg ions. The mass loss evaluation method is simple, but the removal of corrosion products after immersion is a critical issue that must be done with much care. Different methods have been used

to remove the corrosion products at the end of immersion. For example, through rinsing the sample with distilled water [16,32], or by brushing the corrosion debris out from its surface [33]. Also, by cleaning the sample with a chemical such as boiling 15% CrO<sub>3</sub> + 1% AgCrO<sub>4</sub> solution [34]. All these methods have some drawbacks as washing with distilled water cannot remove all the corrosion products leading to some mass gain [16], whilst brushing may destroy the matrix of the metals leaving scratches on its surface which adds to the mass loss. Finally, washing by chemical reagent should be done with much precaution to avoid matrix reaction with the chemical during prolonged washing time. So in order to limit human error, hydrogen evolution method is preferable despite its limitations as well. The weight loss rate ( $\Delta w$ ) in (mg cm<sup>-2</sup> d<sup>-1</sup>) can be expressed as the average corrosion rate ( $p_w$ ) in (mm y<sup>-1</sup>) by the following equality [35]:

$$P_w = 2.10 \Delta w \quad (10)$$

Also, the corresponding corrosion rate ( $P_H$ ) in the same units can be evaluated from  $V_H$  value in mL cm<sup>-2</sup> d<sup>-1</sup> using the following expression [35]:

$$P_H = 2.088 V_H \quad (11)$$

As can be noted from the obtained HE results, the corrosion rate of AXJ530 alloy after 10 h immersion in PBS fluid  $P_H = 5.61$  mm y<sup>-1</sup>, which is in close agreement to that measured from weight loss rate at the same conditions ( $P_w = 5.29$  mm y<sup>-1</sup>). The slight difference between the two values may be related to the method used in removing the corrosion product from the sample surface after the immersion test [16]. On prolonging the immersion time to 96 h, Fig. 1 inset manifests large disagreement between  $P_H$  and  $P_w$  where  $P_w$  surpasses  $P_H$  which becomes five times lower than  $P_w$  ( $P_H/P_w = 0.2$ ). This difference is likely attributed to the relative stabilization of HE rate after ~ 9 h immersion due to the dissolution of some hydrogen in the alloy material. Hydrogen permeation in the solid alloy matrix is easier in PBS tested fluid due to the weak protective surface film formed on its surface, that also offers small resistance to hydrogen ingress into the bulk of the alloy sample [36].

### 3.2. Open circuit potential behavior

Fig. 2 shows the variation of open circuit potential ( $E_{oc}$ ) of the alloy and its base metal in PBS fluid recorded over 96 h exposure. The results clearly demonstrate that in both cases the potential increases rapidly then slowly to reach a more noble value of -1.562 V for the alloy and -1.613 V for pure Mg and later on the potential goes to stabilization after about 12 h and 9 h for the two samples, respectively. This behavior indicates self-healing of material surface caused by its interaction with PBS fluid and deposition of a protective corrosion product layer on its anodic active sites. On the other hand, the small decrease in  $E_{oc}$  value before stabilization indicates a natural tendency of the formed surface layer to dissolve partially at a protracted immersion time.

It is worth to note that, when magnesium material is exposed to an aqueous corrosive environment magnesium hydroxide is first formed as a final corrosion product (Eq. (1)) tending to deposit on the surface if its solubility limit is exceeded ( $K_{sp} = 1.8 \times 10^{-11}$ ) [37]. Therefore, the formation of corrosion product on the sample surface can be attributed to this dissolution-precipitation mechanism. It is also of interest to notice that during the whole testing period the alloy assumes a

cathodic trend compared to the behaviour of its base metal, which is likely related to the difference in the composition and microstructure of the two materials.

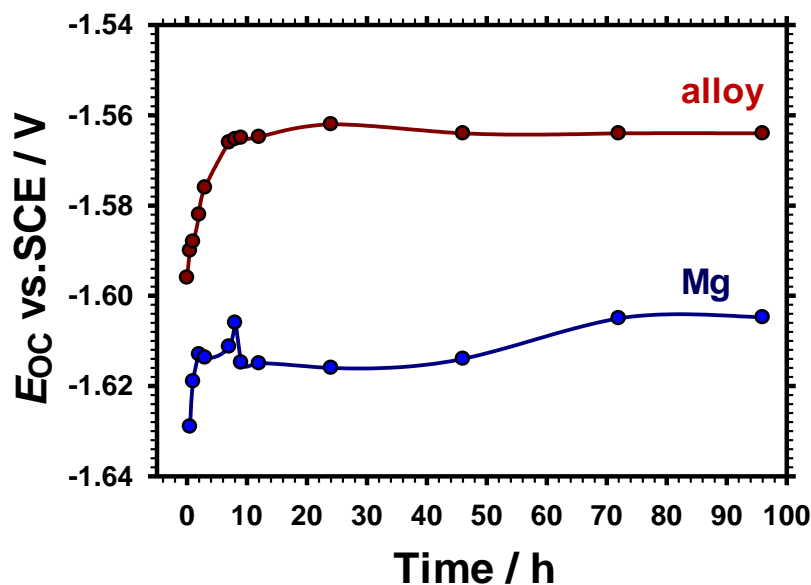


**Figure 2.** Variation with time of OCP (vs. SCE) for pure Mg and AXJ530 alloy in PBS fluid.

### 3.3. Electrochemical impedance spectroscopy

Electrochemical impedance spectroscopy (EIS) is a reasonably non-destructive technique using a minimal perturbative signal and thus is considered as a powerful tool to follow up in real time the corrosion behavior of metallic materials with nearly no surface damage. In these experiments, immersion of Mg and its alloy was carried out continuously in PBS fluid of pH 7.4 at 37 °C, which is used to simulate the biochemical reactions of degradable magnesium materials under physiological conditions. Fig. 3(a-d) presents the impedance spectra (as Bode and Nyquist plots) recorded after different time intervals extended to 96 h in PBS for pure Mg and AXJ530 alloy. The impedance spectra for the two samples display two merged time constants that are typically detected in case of Mg materials [17,37-39]. The spectra on the Bode format (Fig. 3a, c) show two resistive regions at low and high frequency ranges and a capacitive contribution in the middle frequency range that corresponds to a maximum in the phase shift ( $\theta$ ) vs.  $\log f$  plots [40]. As can be seen, the absolute impedance ( $|Z|$ ) at the low frequency range ( $1-10^{-2}$  Hz) experiences a monotonic sharp increase in its value from the incipient time of immersion up to 9 h for Mg (Fig. 3a) and 3 h for the alloy (Fig. 3c), afterwards its value decreases for both materials. A decrease in  $|Z|$  value at long-term immersion reflects a continuous lowering in the interface capacitive behavior [41]. This behavior is commensurate with a shift in the phase maximum ( $\theta_{\max}$ ) to lower and then to higher frequency values during the increasing and decreasing trends in  $|Z|$  value with immersion time. Generally, over the initial three hours of sample immersion the alloy demonstrates better impedance performance than pure Mg. However, on protracting the immersion time, the alloy performance becomes inferior and Mg impedance surpasses

the alloy value. Where at any immersion time > 3 h, values of  $\theta_{\max}$  or  $|Z|$  are always lower for the alloy than those for pure Mg suggesting that the formed corrosion products film on pure Mg in PBS fluid are more stable and offers considerable protection than the one formed on the alloy.

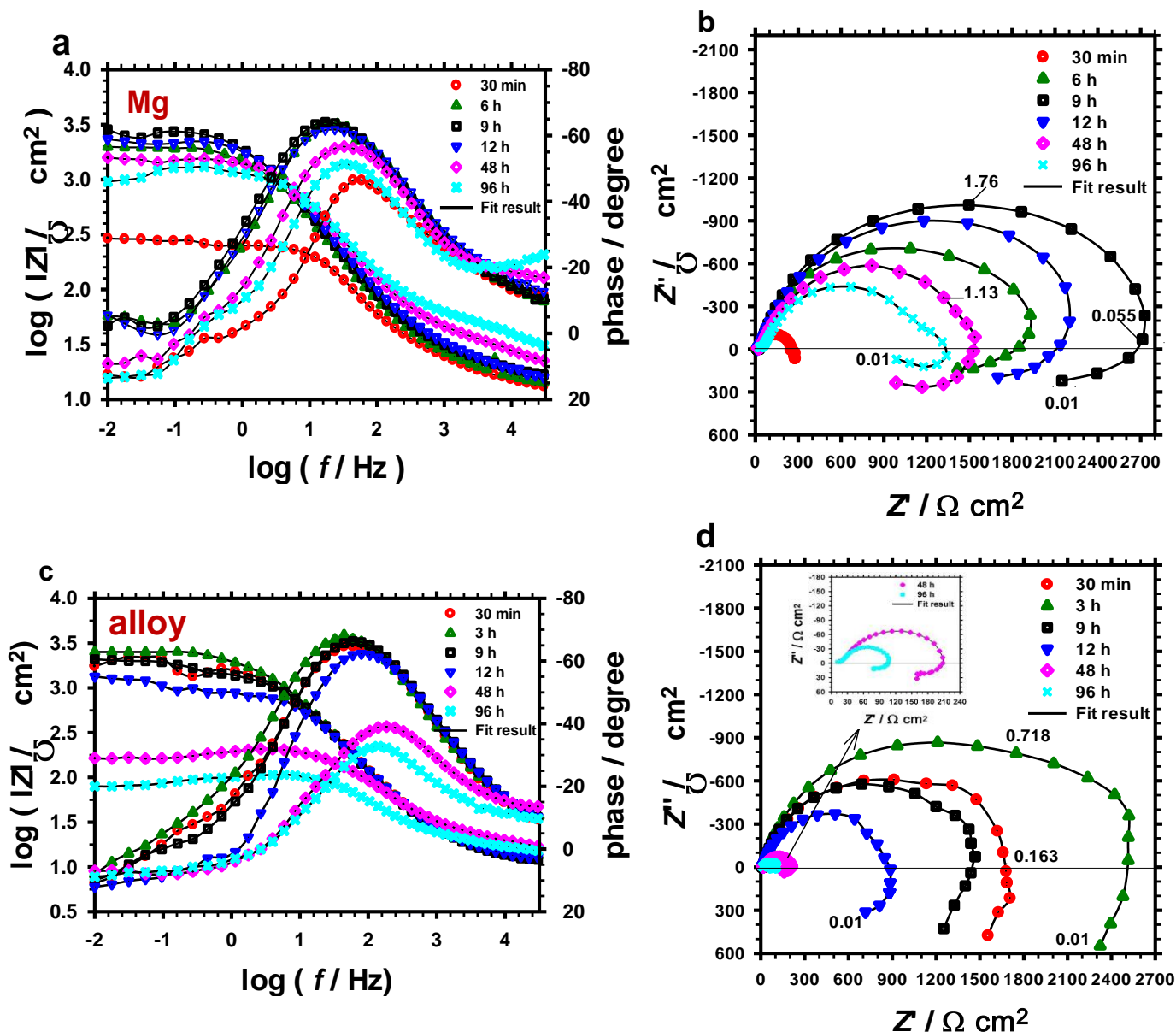


**Figure 3.** Impedance spectra of pure Mg (a & b) and AXJ530 alloy (c & d) as a function of immersion time in PBS fluid at 37 °C: (a & c) Bode plots and (b & d) Nyquist plots.

On the other hand, all Nyquist plots recorded for both pure Mg (Fig. 3b) and the alloy (Fig. 3d) reveal an obvious tendency to form two scarcely depressed capacitive loops, where their diameters increase from the start of immersion time up to 9 h for Mg and 3 h for the alloy followed by shrinking in diameters. This performance agrees well with the behavior of their Bode modules. The results display a feature of two relaxation time constants at HF and LF ranges that vary quantitatively with both of immersion time and electrode material. Furthermore, the EIS spectra of the tested materials are all identical to one another except for the diameters of the loops, indicating similar corrosion

mechanisms in PBS fluid, albeit with different corrosion rates. Rapid corrosion rates of the alloy are likely related to the presence of high concentration of calcium which decrease the corrosion stability due to possible formation of an intermetallic ( $Mg_2Ca$ ) phase on its surface. This phase leads to a significant corrosion rate acceleration induced by the effect of micro-galvanic coupling between  $Mg_2Ca$  and the  $\alpha$ -phase [42,43]. A salient feature in all Nyquist plots obtained herein (Fig. 3b and d) is the display of an inductive behavior with decreasing the frequency at the low domain [44]. The inductive response at low frequencies can be attributed to the relaxation process as originating from the adsorbed/desorbed intermediates or other species in the surface layer on the magnesium alloy [45]. Also, Baril *et al.* [39] have linked the inductive loop to a process involving the univalent  $Mg^+$  cation but without validation or firm evidence for the existence of this univalent cation. However, manifestation of these two opinions may not be possible sometimes and instead the attribution of the appearance of this inductive loop can usually corresponds to surface or bulk relaxation of the adsorbed intermediates or to the formation of unstable salt film as a result of  $Cl^-$  ion incorporation into the surface layer. Indeed, corrosion of a typical polyphasic Mg alloy in most aqueous solutions, especially those containing aggressive  $Cl^-$  ions, is accelerated by the micro-galvanic coupling between the  $\alpha$ -Mg matrix and the second phases. This leads to localized corrosion and pitting which can be virtually noticed on the surface where the surrounding region is relatively shiny and covered by a partially protective film from the corrosion products. In this regard, the evolution of the overall corrosion resistance of the tested samples were quantified by analysing the impedance spectra using the equivalent circuit (EC) shown in Fig. 5 inset, which gave satisfactory fitting results during the overall simulation procedures of the impedance data. The adopted EC model consists from the solution resistance ( $R_s$ ) in series connection to two serial capacitors ( $C_1$  and  $C_2$ ) in parallel with two serial resistances ( $R_1$  and  $R_2$ ). An inductor element ( $L$ ) was also added to express the inductive response at the LF range. In this way, the first time constant ( $R_1C_1$ ) defines the behavior of the system at LF region attributed to the resistance and capacitance of the partially protective layer formed on the sample surface. While the second time constant ( $R_2C_2$ ) describes the behavior of the interface at the base of pores and defects in the surface film. Additionally, in this model a constant phase element (CPE) was used instead of the pure capacitor element ( $C_1$ ) to account for the non-ideal capacitive behavior owing to the surface layer heterogeneity. The conductor element ( $L$ ) is added due to  $Cl^-$  ion adsorption [6,45], as well as to obtain the best fitted results over the whole frequency domain with an average error of less than 0.9%.

The impedance of CPE is defined as:  $Z_{CPE} = 1/Q(j\omega)^\alpha$ , where  $Q$  and  $\alpha$  are independent of frequency and the imaginary number  $j = \sqrt{-1}$ . The admittance of the CPE  $Q$  ( $F\ cm^{-2}\ s^\alpha$ ) will be identical to the real capacitance  $C$  ( $F\ cm^{-2}$ ), at the angular frequency  $\omega = 1$  [40], where  $\omega$  ( $rad\ s^{-1}$ ) =  $2\pi f$  and  $f$  (Hz or  $s^{-1}$ ) is the frequency of the applied ac signal. The deviation parameter  $\alpha$  ( $0 \leq \alpha \leq 1$ ) is an indication of deviation of  $Q$  from  $C$  [40,46]. The appearance of LF time constant ( $R_1C_1$ ) indicates that the formed corrosion products manifest certain degree of porosity as corrosion attack occurs on spots where electrolyte can enter through the pores of the film to the metal surface [23]. All estimated fitted impedance parameters for both AXJ530 alloy and pure Mg as a function of immersion time were collated in Table 3. The microstructure of AXJ530 alloy is shown in Fig. 4b as composed of large primary  $\alpha$ -Mg grains (dark) surrounded by eutectic constituents (light grey). Two types of eutectic

structures can be detected: divorced eutectic and coarse lamellae which forms the majority of the eutectic structure. This coarse lamellae consists of Al- and Ca-rich phase coupled to  $\alpha$ -Mg-rich phase. The Al- and Ca-rich phases were already known as  $(\text{Mg,Al})_2\text{Ca}$  based on TEM and XRD examination [47], Fig. 4b, also shows the presence of  $(\text{Mg,Al})_2\text{Ca}$  and  $\alpha$ -Mg between the large grains of primary  $\alpha$ -Mg. Long precipitates containing calcium and aluminum are found within the primary grains in addition to Mn-Al particles. The composition of Mn-Al particles was found to be close to  $\text{Mn}_4\text{Al}_5$ . Also  $(\text{Mg Al})_2(\text{Ca Sr})$  phase is detected due to the presence of Sr-rich particles between the  $\alpha$ -Mg grain [48] as illustrated in (Fig. 4. inset (e & f)).

**Table 3.** Equivalent circuit impedance parameters of the two tested samples in PBS at 37 °C as a function of immersion time.

Time (h)	$R_1$ ( $\text{k}\Omega \text{ cm}^2$ )	$C_1$ ( $\mu\text{F cm}^{-2}$ )	$\alpha$	$L$ ( $\text{kH cm}^2$ )	$R_2$ ( $\text{k}\Omega \text{ cm}^2$ )	$C_2$ ( $\mu\text{F cm}^{-2}$ )	$R_s$ ( $\Omega \text{ cm}^2$ )
<b>Pure Mg</b>							
0.5	0.09	9.68	0.44	0.28	0.17	45.4	10.4
6	1.68	10.4	0.51	4.02	1.11	51.5	12.4
9	1.97	8.99	0.52	11.5	1.58	49.8	14.9
12	1.77	7.64	0.51	4.88	1.33	46.3	13.3
48	0.62	4.62	0.38	1.88	1.07	31.4	13.8
96	0.53	2.54	0.23	1.13	0.95	23.9	9.60
<b>AXJ530 alloy</b>							
0.5	1.20	9.84	0.68	26.9	0.82	28.8	12.8
3	1.69	10.6	0.61	41.8	1.17	30.1	12.2
9	1.16	9.97	0.63	16.5	0.70	25.1	10.5
12	0.29	9.56	0.59	0.15	0.62	23.4	11.1
48	0.06	9.36	0.50	0.09	0.13	20.2	13.0
96	0.03	8.18	0.53	0.05	0.06	13.3	11.6

As given in Table 3,  $R_s$  is nearly the same for the two tested samples. It is also seen that  $R_1$  and  $R_2$  values are both increased with immersion time up to 9 h for Mg and 3 h only for AXJ530 alloy indicating film healing and development of better protective layer on the sample surface takes place mainly due to formation of a  $\text{Mg}(\text{OH})_2$  corrosion layer. However, with lengthening the immersion period up to 96 h fast deterioration in the surface layer occurs which becomes evident for the alloy than for its base metal. Thus, as it can be seen in Fig. 5, the total resistance of the surface film ( $R_T = R_1 + R_2$ ) increases from 2.02 and 0.26  $\text{k}\Omega \text{ cm}^2$  for the alloy and pure Mg at the commencement of immersion to reach maximum values of 2.86  $\text{k}\Omega \text{ cm}^2$  and 3.55  $\text{k}\Omega \text{ cm}^2$  for AXJ530 alloy and its base metal, respectively. The improvement and self-protection against corrosion for pure Mg can withstand to longer time compared with the alloy. Besides, Fig. 5 reveals that at any immersion period longer than 3 h  $R_T$  value is larger for Mg than for AXJ530 alloy proving that the alloy is less resistant than its base metal in PBS. This suggests that spontaneously formed film on Mg is less porous and therefore more protective than the film formed on the alloy surface.

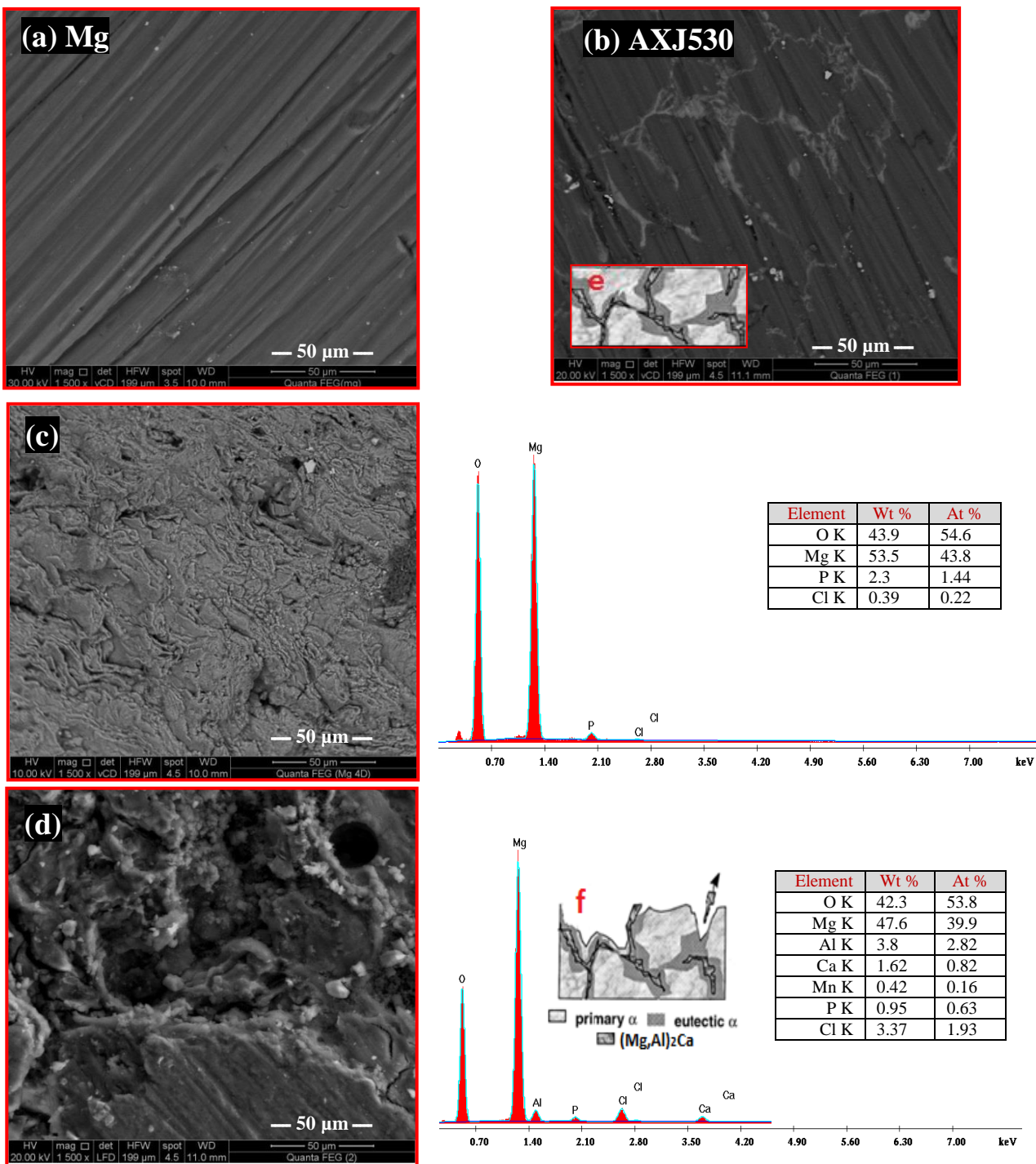


**Figure 4.** SEM micrographs of as-abraded sample surfaces: (a) pure Mg and (b) its alloy. Microstructures and EDX spectra of immersed samples in PBS fluid for 96 h at 37 °C: (c) pure Mg and (d) its alloy. **Inset:** illustration for AXJ530 alloy surface: (e) before immersion and (f) after 96 h immersion.

In fact, the lower corrosion resistance of AXJ530 alloy can be attributed to the lower content of aluminum in primary  $\alpha$ -Mg grains, as well as to the small volume fraction of the cathodic  $(\text{Mg,Al})_2\text{Ca}$  phase that renders it to be disable to act as a good corrosion barrier by forming a continuous network around the  $\alpha$ -Mg matrix. Moreover, isolated and split  $(\text{Mg,Al})_2\text{Ca}$  particles are more disposed to be undermined by the dissolution of neighboring eutectic  $\alpha$ -Mg phase. The sites left by undermined  $(\text{Mg,Al})_2\text{Ca}$  particles constitute possible sealed areas which might favor localized corrosion. On the other hand, the lower passivation behavior of AXJ530 might be also recognized to the discontinuity of the protective  $\text{Mg}(\text{OH})_2/\text{CaH}_2$  or  $\text{Ca}(\text{OH})_2$  corrosion products over the specimen surface, since grain boundaries may cause some defects in the passive film [49].

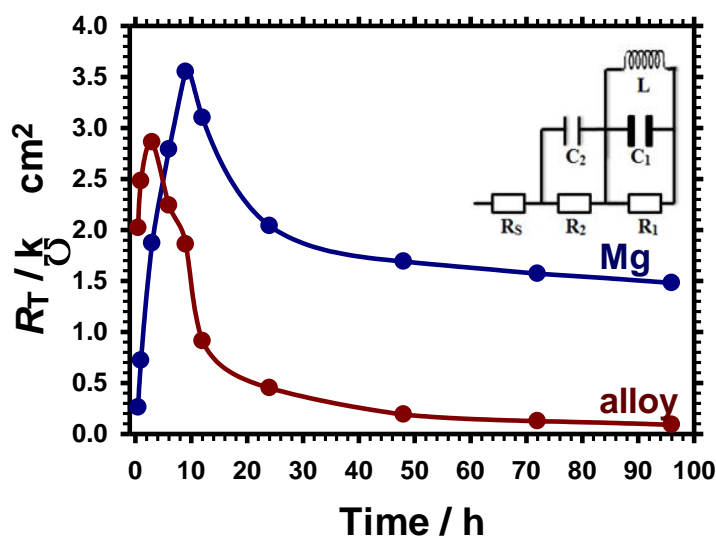


**Figure 5.** Variation with time of the total resistance ( $R_T$ ) for the surface film formed on pure Mg and its alloy immersed in PBS fluid. Inset the electrical equivalent circuit (EC) with two time constants and an inductance element ( $L$ ) which is used to fit the experimental EIS data for the present tested samples.

### 3.3. Potentiodynamic Polarization behavior

Fig. 6 demonstrates potentiodynamic polarization curves of the alloy compared to its base Mg metal after immersion for 96 h in PBS fluid using linear sweep voltammetry scan at a rate of  $2 \text{ mV s}^{-1}$ . Within the potential range from  $-2.2$  to  $-1.0 \text{ V}_{\text{SCE}}$ , it is noticeable that the two Tafel polarization curves ( $E-\log i$ ) of AXJ530 alloy and pure Mg are quite similar. Over the anodic branch, the active potential region terminates directly by a stabilized passivation current zone which ends at a certain transition potential beyond which a sudden increase in the anodic dissolution current is observed [23]. In corrosive environment, this knee point defines the breakdown potential ( $E_b$ ) of a metallic material as being a good indicator for the propensity of its formed anodic passive film in impeding localized corrosion attack [37]. Therefore, over the potential range of the anodic plateau, the metal is in a state of pseudo passivation. As it can be seen in Fig. 6, the alloy achieves breakdown potential ( $E_b$ ) of  $-1.41$

$V_{SCE}$ , whereas Mg has a somewhat more active breakdown potential of  $-1.44 V_{SCE}$ . It follows that the difference ( $\Delta E$ ) between the breakdown potential and the corrosion potential in the anodic region ( $\Delta E = E_b - E_{corr}$ ) for the alloy (150 mV) is much smaller than that for pure Mg (180 mV). This means that the protective passive film formed on Mg sample is less vulnerable to pitting attack in PBS fluid [50] and accordingly has better intrinsic sealing ability when compared with its alloy, most likely due to homogeneous structure of the pure base metal. It is also worth to note that at the corrosion potential ( $E_{corr}$ ) the area of the active anodic regions is limited by the rate of the anodic reaction which attains a relatively steady value [51]. Thus, the corrosion current density ( $i_{corr}$ ) can be often possible from the polarization curves based on the extrapolation of the cathodic Tafel line after  $-50$  mV from  $E_{corr}$ , which assumes to represent the cathodic HE through water reduction via Eq. (4). This method was carried out using Thales software for  $i/E$  analysis provided with the electrochemical workstation. It is also known that  $i_{corr}$  value is inversely related to the polarization resistance ( $R_{pol}$ ) of the sample through Stern–Geary equation by using cathodic and anodic Tafel slopes ( $\beta_c$  and  $\beta_a$ ) as follows [23]:

$$i_{corr} = \frac{\beta_c \beta_a}{2.303(\beta_c + \beta_a)} \cdot \frac{1}{R_{pol}} \quad (12)$$

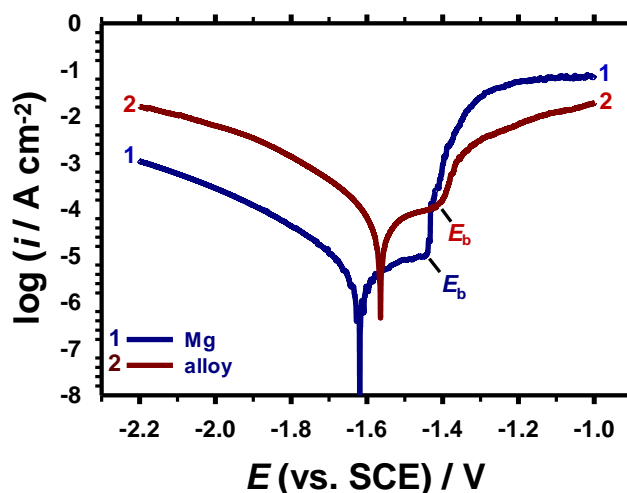


**Figure 6.** Potentiodynamic polarization curves of pure Mg and its alloy after 96 h immersion in PBS fluid at  $37\text{ }^{\circ}\text{C}$ .

Values of  $i_{corr}$  for Mg metal and its alloy samples were estimated to be equal to  $40.3$  and  $238\text{ }\mu\text{A cm}^{-2}$ , respectively. The significantly higher corrosion current density for the alloy ( $\sim 6$  times faster) compared to its pure base metal suggests that the alloy has an inferior corrosion resistance to that for Mg confirming the EIS results. It is also well known that  $i_{corr}$  in  $\mu\text{A cm}^{-2}$  derived from Tafel extrapolation method is related to the average corrosion rate ( $P_i$ ) in  $\text{mm y}^{-1}$  through the correlation [52]:  $P_i = 22.85 i_{corr}$ . Therefore, higher  $i_{corr}$  value means faster degradation rate for the alloy relative to that for its base metal. Besides, Fig. 6 obviously reveals that cathodic polarization current for the alloy is much higher, suggesting a more facile kinetics rate for hydrogen evolution *via* water reduction reaction on the alloy surface than on Mg. In the meanwhile, over the anodic polarization scan and beyond the breakdown potential, the net polarizing current density will be lower for the alloy than for

pure Mg. This is likely attributed to the negative difference effect phenomenon which leads to excessive hydrogen gas evolution on the alloy more than on Mg while anodic metal dissolution is taking place [28].

### 3.4. Surface protection

#### 3.4.1. Fluoride coating

Several methods are reported in the literature for surface modification and coatings in order to control the active degradation of magnesium alloy in biological environments [53]. Among those techniques chemical conversion coating with fluoride has received special attention. The formation of  $\text{MgF}_2$  coating on magnesium and magnesium alloys is an effective way of improving their anti-degradation behavior in simulated physiological fluids. The most effective method for producing thick and consequently more protective  $\text{MgF}_2$  coating is by converting previously prepared  $\text{Mg(OH)}_2$  layer into  $\text{MgF}_2$ . The post fluoride rich deposit depends mainly on the hydroxide layer formation with a defined thickness which is controlled by etching time, NaOH concentration and temperature. Basically, the hydroxide layer controls the thickness of the subsequent fluoride layer formed after immersing in hydrofluoric acid solution [42] in accordance to the following two equations:

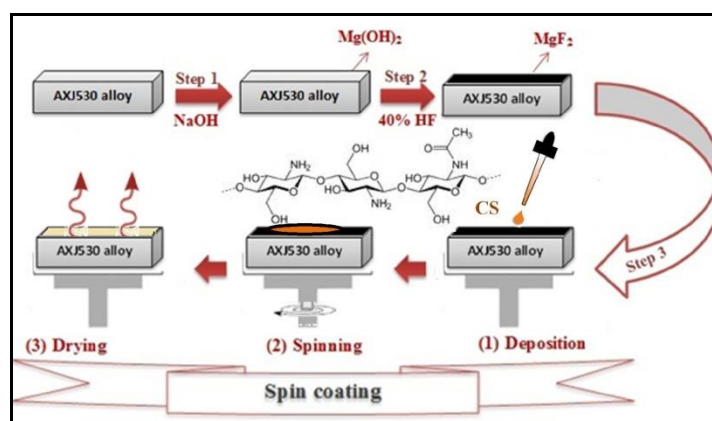
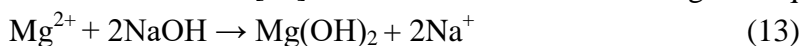


**Figure 7.** Schematic illustration for the CS coating steps.

After forming the fluoride rich ( $\text{MgF}_2$ ) barrier layer, as described in the experimental section, the coated sample was immersed in the test PBS fluid at  $37^\circ\text{C}$  to monitor its impedance spectra with time. Fig. 8a presents the evolution of Nyquist plots for the HF-coated alloy sample, revealing a continuous decrease in the impedance of the coated sample with increasing immersion time. In spite of that, it is obvious that there is a significant reduction in the degradation rate when comparing these results to those in Fig. 3d showing the evolution of Nyquist plots for the bare as-abraded alloy surface.

This is due to creation of fluoride rich layer on the alloy surface by simple chemical conversion of the  $\text{Mg}(\text{OH})_2$  film to a more stable protective barrier layer from  $\text{MgF}_2$  during the HF treatment process. The small electrical conductivity of the formed fluoride layer isolates the magnesium alloy substrate from the electrolyte and ultimately leads to impede the corrosive attack of the prevailing aggressive ions in the medium. Thus, the corrosion of the magnesium/calcium bulk cannot start unless the protective coating is deteriorated. The solubility of magnesium fluoride in aqueous physiological solutions is very low ( $K_{\text{sp}} = 5.16 \times 10^{-11}$ ) and inhibits a fast ion leakage. For this reason, it might be possible to mitigate the degradation of an implant by optimizing the thickness of the protective  $\text{MgF}_2$  layer through controlling the duration of the two pre-treatment steps [42,45].

### 3.4.2. Chitosan coating

The short-term protection provided by the HF treatment attracted the attention of some researchers for its potential as a pretreatment step instead of a final corrosion protection process. The formed  $\text{MgF}_2$  layer on an HF-treated magnesium sample may enable uniform coating formation during subsequent treatment by a sealant as reported in literature [54]. It has been shown by Conceição *et al.*, [55] that polymer coatings on HF-treated magnesium substrates act much better than on substrates with other kinds of pretreatments. This observation was made for different polymers such as poly(ether imide) (PEI) [56], polyacrylonitrile (PAN) [55], polyvinylidene difluoride (PVDF) [54]. In the present study chitosan polymer was chosen on the HF-treated surface of AXJ530 alloy for two main reasons: (i) the insolubility of chitosan in alkaline aqueous solutions can mitigate the degradability of Mg alloy under physiological conditions, and (ii) the degradation products of chitosan after being damaged by enzyme action and hydrolysis are saccharides and glucosamine which may be incorporated into glycoproteins or excreted as carbon dioxide gas during respiration [57]. Chitosan (CS) is an important functional material because of its excellent biocompatibility, biodegradability, high adsorption properties and non-toxicity [58]. It is an alkaline-deacetylated chitin derived from the exoskeletons of insects and shells of crustaceans [59,60]. Fig. 8b displays the evolution of Nyquist plots for spin coated chitosan alloy sample by two successive deposited layers. During the initial stage of immersion, the corrosion resistances in terms of the capacitive loop diameter, is lower than that for the HF-coated sample. Nevertheless, for CS-coated sample it decreases with a much slower rate than for the HF-sample. Fig. 8c clearly shows that the corrosion resistance of the CS-coated sample immersed in PBS for 96 h is higher than that for the HF-coated sample or the uncoated alloy. Chitosan spin coating on the alloy surface with more than two layers was also examined. For the six-layer CS-coated sample, as a typical example, the EIS data depicted in Fig. 8c show no further improvement in the degradation performance of the alloy after 96 h immersion in PBS fluid, most likely due to the appearance of micro-holes and cracks in the thick coat.

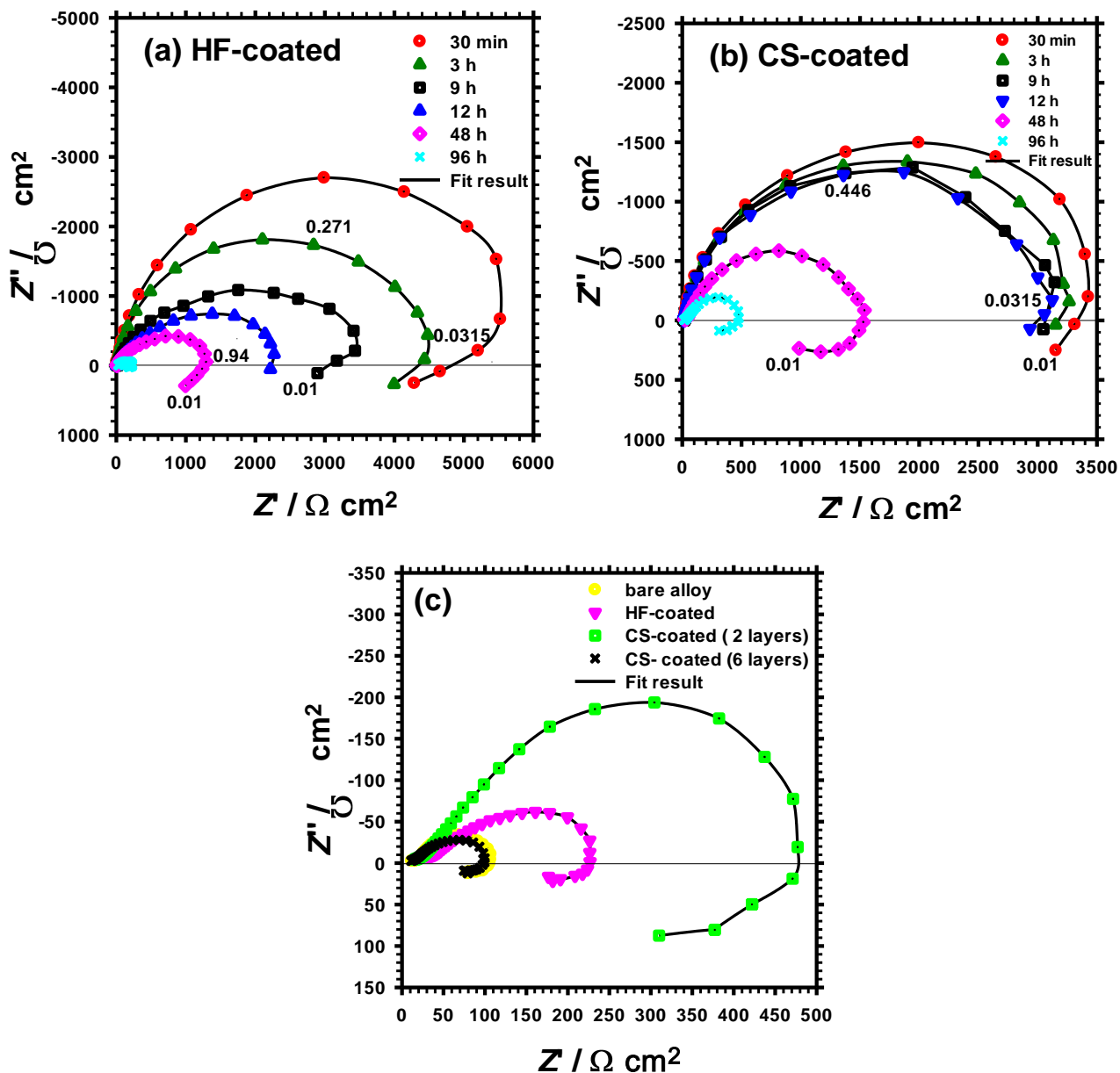


**Figure 8.** Nyquist plots for (a) HF-coated, and (b) CS-coated alloy samples as a function of immersion time in PBS fluid. (c) Comparison of EIS spectra for the different tested samples after 96 h exposure.

The impedance data for both HF-coated and the two-layer CS-coated samples were analyzed and the assessed impedance parameters listed in Table 4 were found to give the best fit with the same EC model shown in Fig. 5 inset. A comparison of the total surface resistance ( $R_T = R_1 + R_2$ ) for the HF-coated and CS-coated samples relative to the uncoated bare alloy after immersion in PBS fluid for different time periods is depicted in Fig. 9. The results reveal that HF coating gives better enhancement in  $R_T$  value of AXJ530 alloy during the short stage of immersion until 9 h, then its value falls relative to the trend for the CS coating. The results clearly demonstrates that over the long stage of immersion CS coating offers superior protection for AXJ530 surface and reduces its degradability, as the total

surface resistance exhibits an enhanced performance until the end of the immersion test which extends to 96 h.

**Table 4.** Equivalent circuit parameters of coated alloy samples in PBS at 37 °C as a function of immersion time.

Time (h)	$R_1$ (k $\Omega$ cm $^2$ )	$C_1$ ( $\mu$ F cm $^{-2}$ )	$\alpha$	$L$ (kH cm $^2$ )	$R_2$ (k $\Omega$ cm $^2$ )	$C_2$ ( $\mu$ F cm $^{-2}$ )	$R_s$ ( $\Omega$ cm $^2$ )
<b>HF-coated alloy</b>							
0.5	2.57	48.8	0.62	42.1	4.9	82.3	4.92
3	2.35	39.4	0.71	32.3	2.40	95.0	7.82
9	1.98	17.3	0.63	30.2	1.89	132.6	8.03
12	1.74	13.8	0.68	0.83	0.79	237.2	7.73
48	0.30	11.6	0.51	0.76	0.22	126.3	8.13
96	0.15	3.4	0.35	0.23	0.09	91.0	16.2
<b>CS-coated alloy</b>							
0.5	1.57	54.46	0.56	27.9	2.79	147.8	12.8
3	1.51	47.92	0.62	50.4	2.44	146.4	13.2
9	1.49	32.82	0.49	16.8	2.42	140.0	12.7
12	1.48	31.10	0.55	14.5	2.40	136.1	12.3
48	0.69	14.62	0.48	1.48	1.07	127.4	12.4
96	0.25	6.50	0.41	0.71	0.43	98.8	10.9

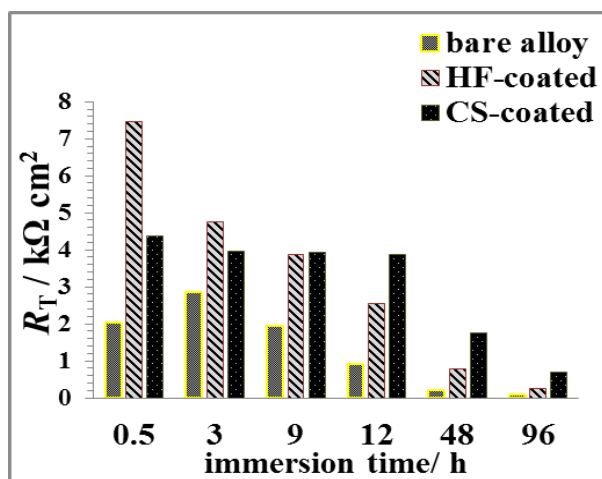


**Figure 9.** The total resistance ( $R_T$ ) of the HF-coated and CS-coated relative to the bare alloy after immersion in PBS fluid for different time periods.

The SEM micrographs and EDX spectra presented in Fig. 10(b–d) after 96 h immersion in PBS fluid are in good agreement with EIS results, where surface of HF-coated and CS-coated samples present a relatively smooth and regular morphology with little cracks, compared to the surface of the uncoated alloy (Fig. 4d). Fig. 10a shows SEM image for HF-coated before immersion.

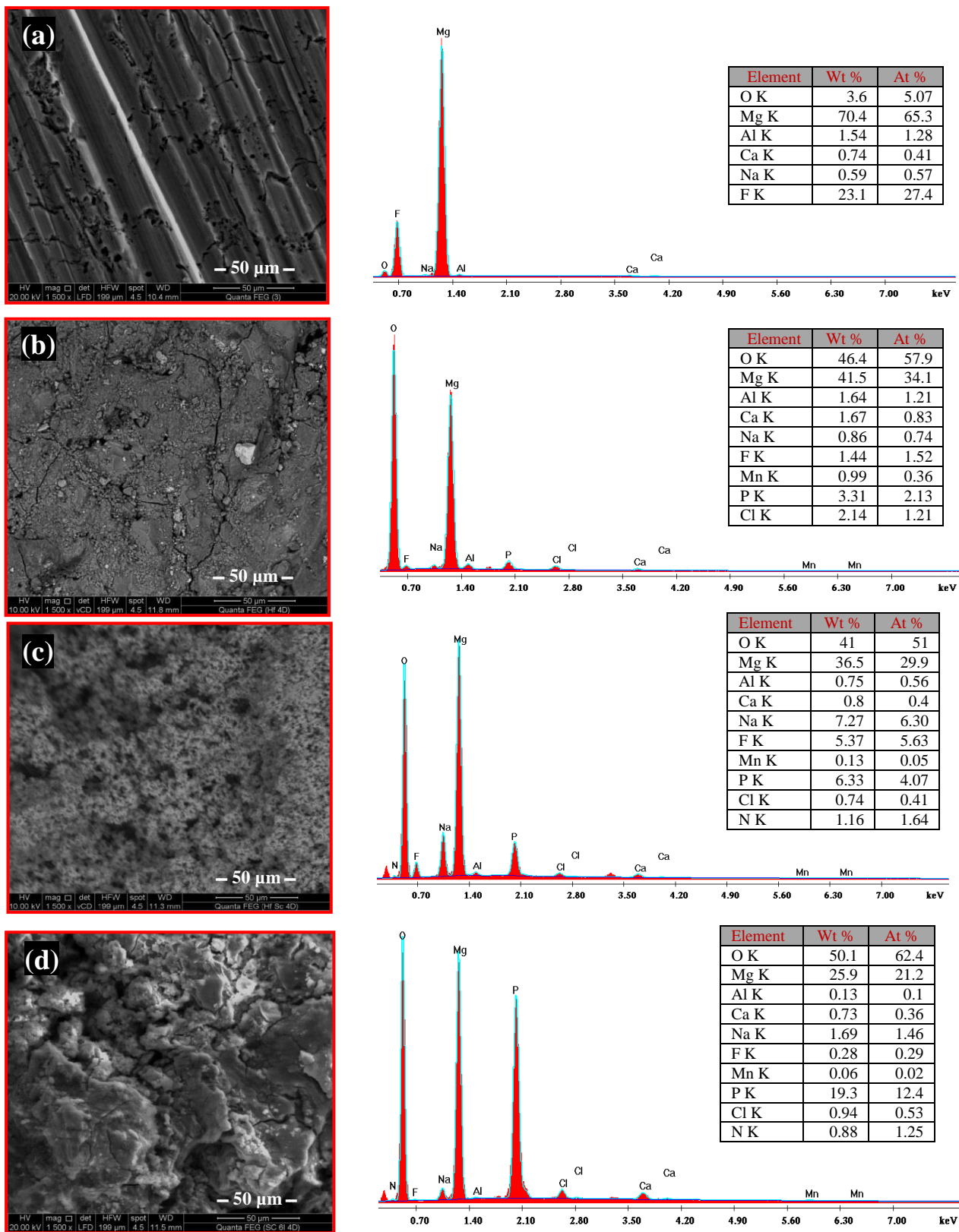


**Figure 10.** SEM micrographs and EDX spectra for: (a) HF-coated alloy sample before immersion and (b - d) coated alloy samples after 96 h immersion in PBS fluid at 37 °C: (b) HF-coated, (c) CS-coated (2 layers) and (d) CS-coated (6 layers).

Potentiodynamic polarization curves were also recorded right after EIS measurements for the bare and coated alloy samples exposed 96 h to PBS fluid at 37 °C as illustrated in Fig. 11. Table 5 shows the electrochemical corrosion parameters derived from those polarization curves. The data correspond to the mean values of the three different specimens tested at each condition. The values of  $i_{\text{corr}}$  and  $\Delta E$  corroborate well with the results obtained from EIS measurements, showing a clear trend for a marked decrease in the degradation rate of the coated specimen versus uncoated one. According to the obtained data, chitosan coating has proven to improve the durability of AXJ530 alloy in PBS fluid.

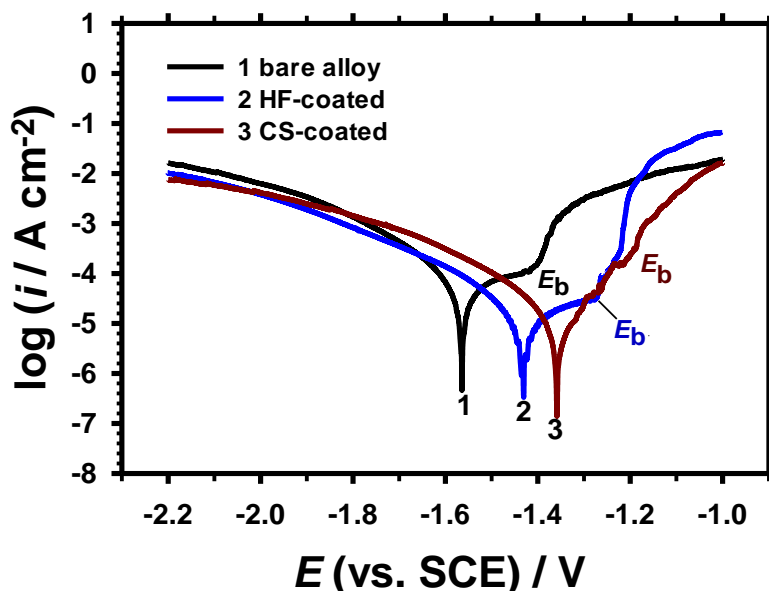


**Figure 11** Potentiodynamic polarization scans for: (1) bare alloy, (2) HF-coated, and (3) CS-coated alloy samples after 96 h immersion in BPS fluid.

**Table 5.** Electrochemical corrosion parameters of bare alloy and coated alloy sample after 96 h immersion in PBS;  $\Delta E = E_b - E_{\text{corr}}$  and  $E_b$  is the breakdown potential.

Sample	$E_{\text{corr}}$ (vs. SCE)	$i_{\text{corr}}$	$\beta_c$	$E_b$ (vs. SCE)	$\Delta E$
	(V)	( $\mu\text{A cm}^{-2}$ )	( $\text{mV dec}^{-1}$ )	(V)	(mV)
Bare alloy	-1.56	238	-357	-1.41	150
HF-coated	-1.43	46.8	-299	-1.27	160
CS-coated	-1.36	42.8	-278	-1.19	170

#### 4. CONCLUSIONS

Various chemical and electrochemical techniques were used to assess the corrosion traits of a novel Ca-Sr-containing magnesium alloy (AXJ530) in phosphate buffer saline fluid (pH 7.4) at 37 °C. At short stage of immersion, the results showed self-healing and passivation extending up to 3 h for the alloy and 9 h for pure Mg. However, at time higher than 3 h, EIS data showed that the alloy exhibits

lower total surface resistance ( $R_T$ ) compared with its base metal mainly due to the micro-galvanic coupling effect. This finding is in good agreement with the Tafel polarisation results as marked by higher corrosion current density ( $i_{\text{corr}}$ ) and lower breakdown potential ( $E_b$ ) for the alloy than those for Mg. To slow down the degradability of the alloy and hence improve its performance and biocompatibility in the physiological environment, fluoride rich coated layer was formed on its surface by two-step treatment method with NaOH and HF. Further treatment by chitosan polymer using spin coating technique was also applied to mitigate its degradation rate. The electrochemical results manifest that the corrosion resistance in term of  $R_T$  value for HF-coated and CS-coated samples are always higher than those for the as-abraded AXJ530 alloy. Generally, HF-coating gives better improvement in the overall corrosion resistance of the alloy during the early stage of immersion until 9 h. After that its resistance falls down relative to the CS-coating which offer a relatively good enhancement in the  $R_T$  value of the alloy during the long term immersion for 96 h. It is also observed that  $i_{\text{corr}}$  is significantly reduced for HF-coated and CS-coated samples compared to the uncoated alloy value. According to the data obtained, chitosan coating successfully improves the durability of AXJ530 magnesium alloy in PBS fluid which paves the way for a possible control of its performance as a potential biodegradable medical implant.

#### ACKNOWLEDGEMENT

Facilities provided by Chemistry Department, Faculty of Science, Cairo University are highly appreciated. Also, the authors would like to thank Dr. A. Ghanem, researcher at National Research Centre (NRC), Giza, Egypt, for the accessibility to the spin coating system.

#### References

1. M. P. Staiger, A.M. Pietak, J. Huadmai and G. Dias, *Biomaterials*, 27 (2006) 1728
2. Y. Zhang, S. Wu, Q. Chen, X. Zhou and Z. Wei, *Int. J. Electrochem. Sci.*, 10 (2015) 1015
3. X. -N. Gu and Y.-F. Zheng, *Front. Mater. Sci. China*, 4 (2010) 111.
4. T. Okuma, *Nutrition*, 17 (2001) 679.
5. C. Feillet-Coudray, C. Coudray, F. Wolf, J. Henrotte, Y. Rayssiguier and A. Mazur, *Metabolism*, 53 (2004) 660
6. L. Wang, T. Shinohara and B. -P. Zhang, *J. Solid State Electrochem.*, 14 (2010) 1897
7. F. Witte, V. Kaese, H. Haferkamp, E. Switzer, A. Meyer-Lindenberg, C. Wirth and H. Windhagen, *Biomaterials*, 26 (2005) 3557-3563.
8. Z. Li, X. Gu, S. Lou and Y. Zheng, *Biomaterials*, 29 (2008) 1329.
9. K. Oh-Ishi, R. Watanabe, C. Mendis and K. Hono, *Mater. Sci. Eng. A*, 526 (2009) 177.
10. B. R. Powell, A. A. Luo, V. Rezhets, J. J. Bommarito and B. L. Tiwari, *SAE Technical Paper*, 110 (2001) 406.
11. B. R. Powell, V. Rezhets, A. A. Luo and B. L. Tiwari, *USA Patent*, No. 6264763 B1. (2001)
12. M. Liu and G. -L. Song, *Corros. Sci.*, 77 (2013) 143.
13. H. Zhao, S. Cai, Z. Ding, M. Zhang, Y. Li and G. Xu, *RSC Adv.*, 5 (2015) 24586.
14. T. Zhang, Y. Shao, G. Meng, Y. Li and F. Wang, *Electrochim. Acta*, 52 (2006) 1323
15. X. Gu, W. Zheng, Y. Cheng and Y. Zheng, *Acta Biomater.*, 5 (2009) 2790.
16. F. Witte, J. Fischer, J. Nellesen, H. -A. Crostack, V. Kaese, A. Pisch, F. Beckmann and H. Windhagen, *Biomaterials*, 27 (2006) 1013.
17. A. Alabbasi, S. Liyanaarachchi and M. B. Kannan, *Thin Solid Films*, 520 (2012) 6841

18. Q. Xu, Y. Liu, C. Liu, A. Tian, X. Shi, C. Dong, Y. Zhou and H. Zhou, *RSC Adv.*, 5 (2015) 14458
19. M. Thomann, C. Krause, N. Angrisani, D. Bormann, T. Hassel, H. Windhagen and A. Meyer-Lindenberg, *J. Biomed. Mater. Res. Part A*, 93 (2010) 1609
20. L. Xu and A. Yamamoto, *Colloids Surf., B* 93 (2012) 67
21. F. J. Pavinatto, L. Caseli and O. N. Oliveira Jr, *Biomacromolecules*, 11 (2010) 1897
22. A. Niemczyk and M. El Fray, *Prog. Chem. Appl. Chitin Deriv.*, 18 (2013) 59
23. F. El-Taib Heakal, O. Shehata and N. Tantawy, *Corros. Sci.*, 86 (2014) 285.
24. A. Niemczyk, P. Kaczorowski and M. El Fray, *Prog. Chem. Appl. Chitin Deriv.*, (2015) DOI: 10.15259/PCACD.20.23.
25. G. Frankel, A. Samaniego and N. Birbilis, *Corros. Sci.*, 70 (2013) 104.
26. F. Cao, Z. Shi, J. Hofstetter, P. J. Uggowitzer, G. Song, M. Liu and A. Atrens, *Corros. Sci.*, 75 (2013) 78.
27. N. Birbilis, A. King, S. Thomas, G. Frankel and J. Scully, *Electrochim. Acta*, 132 (2014) 277
28. G. Song and A. Atrens, *Adv. Eng. Mater.*, 5 (2003) 837.
29. G. He, Y. Wu, Y. Zhang, Y. Zhu, Y. Liu, N. Li, M. Li, G. Zheng, B. He and Q. Yin, *J. Mater. Chem. B*, 3 (2015) 6676.
30. M. Bornapour, N. Muja, D. Shum-Tim, M. Cerruti and M. Pektugulyuz, *Acta biomaterialia*, 9 (2013) 5319.
31. Y. Xin, C. Liu, X. Zhang, G. Tang, X. Tian and P. K. Chu, *J. Mater. Res.*, 22 (2007) 2004.
32. Y. Wang, M. Wei and J. Gao, *Mater. Sci. Eng. C*, 29 (2009) 1311.
33. M. Schinhammer, A.C. Hänzi, J.F. Löffler and P.J. Uggowitzer, *Acta Biomater.*, 6 (2010) 1705.
34. W. Zhou, T. Shen and N. N. Aung, *Corros. Sci.*, 52 (2010) 1035.
35. S. Johnston, Z. Shi and A. Atrens, *Corros. Sci.*, 101 (2015) 182.
36. K. Nogita, S. Ockert, J. Pierce, M. Greaves, C. Gourelay and A. Dahle, *Int. J. hydrogen energy*, 34 (2009) 7686.
37. G. Wu, Y. Zhao, X. Zhang, J. M. Ibrahim and P. K. Chu, *Corros. Sci.*, 68 (2013) 279
38. X. -W. Guo, J. -W. Chang, S. -M. He, W. -J. Ding and X. Wang, *Electrochim. Acta*, 52 (2007) 2570.
39. G. Baril, C. Blanc and N. Pébère, *J. Electrochem. Soc.*, 148 (2001) B489.
40. F. El-Taib Heakal, O. Shehata and N. Tantawy, *Corros. Sci.*, 56 (2012) 86.
41. J. R. McDonald, *Impedance spectroscopy: emphasizing solid materials and systems*, John Wiley & Sons Inc., New York, USA (1987).
42. A. Drynda, T. Hassel, R. Hoehn, A. Perz, F.W. Bach and M. Peuster, *J. Biomed. Mater. Res. A*, 93 (2010) 763.
43. H. R. Bakhsheshi-Rad, M. Abdellahi, E. Hamzah, A. F. Ismail and M. Bahmanpour, *J. Alloys Compd.*, 687 (2016) 630.
44. A. King, N. Birbilis and J. Scully, *Electrochim. Acta*, 121 (2014) 394.
45. M. C. Turhan, R. Lynch, M. S. Killian and S. Virtanen, *Electrochim. Acta*, 55 (2009) 250.
46. T. Ishizaki, J. Hieda, N. Saito, N. Saito and O. Takai, *Electrochim. Acta*, 55 (2010) 7094.
47. A. Suzuki, N. Saddock, J. Jones and T. Pollock, *Scr. Mater.*, 51 (2004) 1005
48. S. Amira, D. Dubé, R. Tremblay and E. Ghali, *Mater. Character.*, 59 (2008) 1508
49. E. E. Stansbury and R. A. Buchanan, *Fundamentals of electrochemical corrosion*, ASM international, Ohio, USA, (2000).
50. H. Jia, X. Feng and Y. Yang, *Corros. Sci.*, 120 (2017) 75
51. M. Curioni, F. Scenini, T. Monetta and F. Bellucci, *Electrochimica Acta*, 166 (2015) 372.
52. M. E. Turan, Y. Sun, Y. Akgul, Y. Turen and H. Ahlatci, *J. Alloys Compd.*, 724 (2017) 14
53. H. Hornberger, S. Virtanen and A. Boccaccini, *Acta Biomater.*, 8 (2012) 2442

54. T. Da Conceicao, N. Scharnagl, C. Blawert, W. Dietzel and K. Kainer, *Thin Solid Films*, 518 (2010) 5209
55. T. F. da Conceição, N. Scharnagl, W. Dietzel and K. U. Kainer, *Corros. Sci.*, 62 (2012) 83.
56. T. F. da Conceicao, N. Scharnagl, W. Dietzel and K. Kainer, *Corros. Sci.*, 53 (2011) 338.
57. X. Gu, Y. Zheng, Q. Lan, Y. Cheng, Z. Zhang, T. Xi and D. Zhang, *Biomed. Mater.*, 4 (2009) 044109.
58. M. Dash, F. Chiellini, R. Ottenbrite and E. Chiellini, *Prog. Polym. Sci.*, 36 (2011) 981.
59. S. Naficy, J. M. Razal, G. M. Spinks and G. G. Wallace, *Sens. Actuators, A*, 155 (2009) 120.
60. D. Depan, A. P. Kumar and R. P. Singh, *Acta Biomater.*, 5 (2009) 93.

© 2018 The Authors. Published by ESG ([www.electrochemsci.org](http://www.electrochemsci.org)). This article is an open access article distributed under the terms and conditions of the Creative Commons Attribution license (<http://creativecommons.org/licenses/by/4.0/>).